A model of fracture nucleation, growth and arrest, and consequences for fracture density and scaling

Philippe Davy, Romain Le Goc, Caroline Darcel

▶ **To cite this version:**

A model of fracture nucleation, growth and arrest, and consequences for fracture density and scaling

Philippe Davy,[1] Romain Le Goc,[2] and Caroline Darcel[2]

[1]   In order to improve discrete fracture network (DFN) models, which are increasingly required into groundwater and rock mechanics applications, we propose a new DFN modeling based on the evolution of fracture network formation—nucleation, growth, and arrest—with simplified mechanical rules. The central idea of the model relies on the mechanical role played by large fractures in stopping the growth of smaller ones. The modeling framework combines, in a time-wise approach, fracture nucleation, growth, and arrest. It yields two main regimes. Below a certain critical scale, the density distribution of fracture sizes is a power law with a scaling exponent directly derived from the growth law and nuclei properties; above the critical scale, a quasi-universal self-similar regime establishes with a self-similar scaling. The density term of the dense regime is related to the details of arrest rule and to the orientation distribution of the fractures. The DFN model, so defined, is fully consistent with field cases former studied. Unlike more usual stochastic DFN models, ours is based on a simplified description of fracture interactions, which eventually reproduces the multiscale self-similar fracture size distribution often observed and reported in the literature. The model is a potential significant step forward for further applications to groundwater flow and rock mechanical issues.

Citation: Davy, P., R. Le Goc, and C. Darcel (2013), A model of fracture nucleation, growth and arrest, and consequences for fracture density and scaling, *J. Geophys. Res. Solid Earth*, *118*, 1393–1407, doi:10.1002/jgrb.50120.

1.   Introduction

[2]   Fractures are ubiquitous in geological systems and key structures for groundwater flow and mechanical resistance of rocks. It is now clearly demonstrated that the density of fractures and their spatial organization are controlling flow and mechanical properties of rock masses. Thus, most of the predictions in hydrogeology, seismology, and geomechanics—with application to water resources, mining, geothermal industry, deep waste isolation, among others—are dependent on the pertinence of the fracture network description, although the degree to which it must be is still an issue [*Berkowitz et al.*, 2000b; *Caumon et al.*, 2009; *de Dreuzy et al.*, 2001a, b; *Paluszny and Matthai*, 2010; *Svensson*, 2001].

[3]   An intrinsic difficulty is to deal with a range of fracture scales that cover several orders of magnitudes in any tectonic system, from microfractures smaller than micro- to millimeters to tectonic faults larger than hundreds of meters to kilometers. The apparent similarity between fracture patterns at different scales has long been recognized by geologists [*Tchalenko*, 1970] and has led to apply fractal scaling concepts to fracture networks: fracture patterns are likely characterized by fractal dimensions; fracture length distributions appear to be adequately fitted by power laws (the only mathematical functions that do not require a scale parameter) from meter to tens of kilometer scales [see the compilation by *Bonnet et al.*, 2001]. Whatever the model of fracture organization is, taking account of this large range of fracture scales in mechanical or flow models requires either high-resolution underground imagery of fracture networks or the development of pertinent stochastic fracture network models to replace the lack of observation. Since the former is still out of reach, most models of fluid flow and transport processes are based on Statistical Discrete Fracture Network methods (DFN) [see *Jing et al.*, 2007 for a review], which are statistical generation methods conditioned to length and orientation frequency distribution. The positions of fractures are generally assumed to be random, but this assumption needs to be further proven since it does not reflect the complexity of geological patterns [*Ackermann and Schlische*, 1997; *Darcel et al.*, 2003a].

[4]   The aim of this paper is to develop a stochastic DFN modeling framework able to match both important properties that constitute a large part of the complexity of geological fracture networks: the fracture-to-fracture spatial interactions and the scaling relationships between fracture lengths and densities over several orders of magnitude. Both are critical for defining the DFN connectivity [*Berkowitz et al.*, 2000a;

[1]Geosciences Rennes, CNRS, University of Rennes 1, Campus de Beaulieu, Rennes, France.

[2]ITASCA Consultants, SAS, 64 chemin des Mouilles, Ecully, France.

Corresponding author: P. Davy, Geosciences Rennes, CNRS, University of Rennes 1, Campus de Beaulieu, Rennes, France. (philippe.davy@univ-rennes1.fr)

Bour and Davy, 1997, 1998; *Darcel et al.*, 2003b; *Davy et al.*, 2006a; *de Dreuzy et al.*, 2001a]. The method we develop is based on a simplified modeling of the fracturing processes, which still enables handling millions of fractures in 3D. It relies on the main stages of fracture evolution: nucleation, growth, and arrest. This time-wise process differs from classical DFN models that only "bootstrap" the current geological stage.

[5] The basic mechanical concepts are derived from the "likely" universal model of fracture scaling (UFM) of [*Davy et al.*, 2010], which theoretically derives a fracture-size density distribution model from simplified rules of fracture arrest. The model, which depends only on the topological network dimension D and on a dimensionless parameter γ, was found to be a good fit for a large number of fracture datasets, whether they are made of faults or joints. The basic idea is to highlight the mechanical role of large fractures in stopping the growth of smaller ones. A strict causality rule—*a small fracture cannot cross a larger one, but the reverse is likely to occur*—obviously simplifies the mechanical reasons for stopping fracture growth [*Crampin*, 1994, 1999; *Pollard and Aydin*, 1988; *Renshaw and Pollard*, 1994; *Renshaw and Park*, 1997; *Renshaw et al.*, 2003], but it renders the main mechanical interactions [*Nur*, 1982; *Segall and Pollard*, 1983; *Spyropoulos et al.*, 1999] and is statistically consistent with the large number of commonly observed T-like fracture intersections. Additionally and pragmatically, it is easily manageable in simple stochastic models. *Davy et al.* [2010] demonstrated that this pseudo-mechanical rule entails a quasi-universal density distribution of fracture sizes, which takes the form of a power law with a fixed exponent and a quasi-fixed density term. The reason why this universal distribution emerges is that the fracture length once arrested is about the distance to its larger neighbor. This geometrical rule fixes the density of large fractures. If fractures are smaller than the distance to the nearest neighbor, they are not suppose to interact mechanically, and their length distribution is then controlled by the growth law of isolated fractures (dilute regime).

[6] *Davy et al.* [2010] show that this two-regime length distribution is consistent with the statistics derived from a few detailed mapping studies of natural outcrops or experiments, with a transition between the "dense" large-length UFM distribution and the "dilute" small-length one that was observed to vary from 1–10 m for joint networks to ~20 km for the San Andreas fault system. They also show that this so-called UFM generation model leads to networks, the connectivity and flow properties of which are significantly different from the classical random (Poisson statistics) model, even if the fracture length distributions are identical. This emphasizes the need to develop this kind of DFN models that mimic fracturing processes.

[7] In this paper, we discuss possible nucleation, growth, and arrest rules that "naturally" generate the scaling laws observed in fracture networks. As in *Davy et al.* [2010], we use the fracture-length density distribution $n(l, L)$ as the statistical descriptor of fracture patterns. $n(l, L)$ dl is the number of fractures of length in the range $[l, l+\mathrm{d}l]$ within a volume of typical size L. For geological fracture networks, $n(l, L)$ has been found to be adequately fitted by the following scaling laws valid over a large range of scales:

$$n(l, L) = \alpha \ l^{-a} L^{D}, \tag{1}$$

where D is formally the mass (or correlation) dimension of the fracture-center network that is smaller or equal to the topological dimension [see *Bonnet et al.*, 2001; *Bour et al.*, 2002 for more explanations]; a is the power-law length scaling exponent, and α a the density term that is likely increasing during fracture growth.

[8] Note that this paper is the first step towards a complete DFN methodology that can be applied to the modeling of flow and mechanical properties of fracture-controlled geologic sites. Such applications require additional information on fracture aperture (for hydraulic properties), strength, and elastic parameters (mechanical properties) that we do not discuss in this paper. It is no insignificant matter, considering the critical role of fracture transmissivity distribution on the macroscopic flow and transport properties [*de Dreuzy et al.*, 2001a, 2001b, 2002; *de Dreuzy et al.*, 2010].

2. The Complete Model of Fracture Formation: Nucleation, Growth, and Arrest

[9] Fracturing is a feedback-loop process where the growth of fractures modifies their growth properties (through elastic stresses within the unfractured material) [*Atkinson*, 1987; *Bourne and Willemse*, 2001; *Ingraffea*, 1987; *Kachanov and Laures*, 1989; *Pollard and Aydin*, 1988; *Segall*, 1984a,1984b]. The complexity of this dynamic process is directly related to the complexity of the developing network structure. This (somewhat trivial) statement illustrates the difficulty to simplify a process that leads in nature to networks with fracture sizes spanning over orders of magnitudes [*Bonnet et al.*, 2001].

[10] In addition to describing the geometry and scaling properties of fractured systems, a DFN description is also relevant to analyze the main mechanical interactions of fracture networks that are basic to define fracture growth [*Kachanov and Laures*, 1989; *Kachanov*, 2003]. Although less versatile than a continuum-mechanics approach (some assumptions about the shape of fractures and the homogeneity of elastic properties are required to solve the mechanical problem), the DFN is particularly well suited to describe the three main stages of the complete fracture formation stages—(i) nucleation of fractures, (ii) growth, that is, propagation of fractures, and (iii) fracture arrest—and to analyze the properties of the resulting network.

[11] A few studies have put emphasis on the relationship between the different elements of the fracturing stages and the produced fracture density distributions, considering either a full mechanical description of the second and third stages [*Cowie et al.*, 1993; *Cowie et al.*, 1995; *Hardacre and Cowie*, 2003; *Kamaya and Kitamura*, 2004; *Malthe-Sørenssen et al.*, 1998; *Olson*, 1993; *Renshaw and Pollard*, 1994; *Renshaw*, 1996] or simplified rules [*Josnin et al.*, 2002]. The former gives obviously a better description of the physical processes; however, numerical simulations are time consuming, and the complexity of the simulated networks is far to reach those of natural systems in terms of process dimension (most of them are considering 2D growing fractures with plane strain hypothesis), fracture orientations, or range of fracture scales (Figure 1).
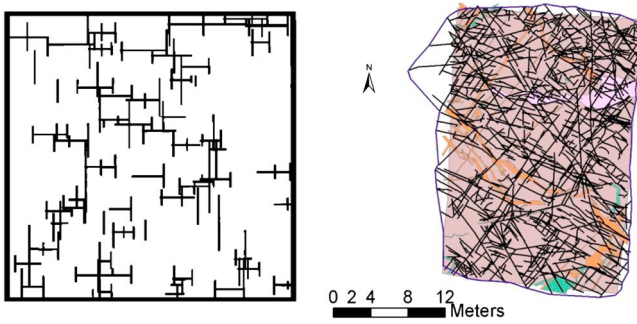
Figure 1. Fracture networks obtained from numerical simulations [Renshaw, 1996] and mapped from granitic outcrop (Forsmark, Sweden) [*SKB*, 2004a].

[12] In the following paragraphs, we discuss the different rules and functions for the 3D network evolution, and we test the relationship between the fracturing rules and the fracture length distribution at any stage of the fracturing history. The time scales to produce these networks in geological systems is quite long, from several thousand to million years [*Walsh et al.*, 2002], entailing that the laws discussed in the next paragraphs are averaging many of the details of the fracturing process including the seismic cycle.

2.1. Nucleation

[13] Nucleation of fractures is a complex process both controlled by the repartition of flaws in matter (pores, grain boundaries, cleavage planes, etc.) [*Engelder*, 1987; *Tapponnier and Brace*, 1976] and by mechanical controls that make nuclei active or not [*Betekhtin and Kadomtsev*, 2005; *Ingraffea*, 1987; *Knauss*, 1969]. This results in a microcrack damaging that eventually leads to the formation of faults or joints [*Ashby and Sammis*, 1990; *Kranz*, 1983; *Reches and Lockner*, 1994; *Segall and Pollard*, 1983]. In the following, we use the term "nuclei" to name the flaws that can be considered as growing cracks and "flaws" those that are not yet activated or growing much slower than cracks of same characteristics.

[14] In the most simplistic cases, former studies assumed that the material contains a certain number of randomly distributed nuclei of about constant length that grows concurrently to form the eventual fracture network [*Olson*, 1993; *Renshaw and Pollard*, 1994; *Renshaw*, 1996]. More complex models also allow flaws to be active as nuclei for further crack growth [*Ashby and Sammis*, 1990; *Betekhtin and Kadomtsev*, 2005; *Reches and Lockner*, 1994; *Tapponnier and Brace*, 1976]. The reason why nuclei forms is likely related to stress redistribution by growing cracks, stress increase, thermal activation, chemical corrosion, etc. [*Atkinson and Meredith*, 1981; *Betekhtin and Kadomtsev*, 2005; *Buchel and Sethna*, 1997; *Hamiel et al.*, 2006; *Horii and Nemat-Nasser*, 1985; *Reches and Lockner*, 1994; *Sethna*, 2001]. The feedback loop between fracture nucleation and growth due to stress redistribution can result in strikingly different geometries of the eventual fracture pattern, depending on the initial distribution of weak and strong area defects [*Alava et al.*, 2006; *Davy et al.*, 1995; *Hansen et al.*, 1991; *Herrmann and Roux*, 1990]. Such a

complexity is beyond the scope of this study (see however the discussion): we aim at simulating networks from simple geometrical rules rather than time-consuming mechanical calculations. However, the correlations between nucleation, growth, and existing fracture patterns, which are emphasized in the previously cited studies, are likely an improvement of the current modeling and should be considered in further studies.

[15] In the following, we assume that in the intact rock, nuclei are uniformly distributed both in terms of orientations and positions. The nature of the nuclei length distribution $p_N(l)$ is not a critical point as long as the nuclei are small. We consider both exponential and power-law distributions for $p_N(l)$:

$$p_N(l) = \frac{1}{l_N} \exp\left(-\frac{l}{l_N}\right) \tag{2}$$

$$p_N(l) = \frac{1-b}{l_N}\left(\frac{l}{l_N}\right)^{-b}, \tag{3}$$

where l is the nuclei size, and l_N is a characteristic length scale, which is the average nuclei size for the exponential distribution, and the lower bound of the distribution for the power-law distribution (in this case, the average length is $\frac{b-1}{b-2}l_N$), and b an exponent.

[16] Finally, we consider two end-member cases where all nuclei are present in the system with no nucleation, or where the nucleation appearance rate is constant. The number of nuclei is noted n_N, and the nucleation appearance rate is its time (t) derivative $\dot{n}_N = \frac{dn_N}{dt}$.

2.2. Fracture Propagation

[17] Fracture growth is an energy-consuming process that involves (at least) the creation of new fracture surfaces, the work done against friction (for modes II and III), and the creation and deformation of the inelastic process zone nearby the fracture tip [*Cowie and Scholz*, 1992a,1992b; *Vermilye and Scholz*, 1998]. Open cracks in mode I are potentially unstable—once the crack length is larger than a critical value, the crack is likely propagating at wave speed up to the system limits—but stable growth mode is expected for mode-II faults, strain-rate or controlled conditions (unlike constant applied remote stress), or subcritical growth [*Atkinson and Meredith*, 1987; *Atkinson*, 1982, 1984; *Cowie and Scholz*, 1992a; *Segall and Pollard*, 1983]. Most of these "stable" cases are likely to occur in natural geological environment [*Schultz*, 2000; *Segall and Pollard*, 1983], although the question whether a Griffith-type instability instead of a quasi-static growth exists is still debated for geological tensile cracks under constant stress [*Olson and Schultz*, 2011; *Scholz*, 2010].

[18] In the following, we only consider subcritical-like fracture growth, where the fracture growth speed is dependent on fracture length. In addition to its geological relevance, the case allows us to highlight the close relationship between the length distribution and the growth law as demonstrated below. Extrapolation to models where the fracture growth is independent of fracture length is rather straightforward.

[19] The general form of the growth law in the subcritical regime is still an issue. Most of the experimental data on rock

samples have been obtained for mode I [*Atkinson*, 1984], and only a few for modes II and III [*Ko and Kemeny*, 2011] with results consistent with mode I. The main fitting or theoretical models are either power law or exponential model.

[20] The power law was introduced by *Charles* [1958] (and known as the Charles' law) and widely used in the literature to describe the crack tip velocity in the subcritical regime: $v = \frac{dl}{dt} = CK^m$ [*Atkinson*, 1984; *Das and Scholz*, 1981; *Kamaya and Kitamura*, 2004; *Newman and Raju*, 1981], where K is the stress intensity factor, and m is the stress-corrosion index or the subcritical fracture growth index. m can vary widely and depends on the fracture growth mechanism and rock type [*Atkinson*, 1987]. *Olson* [2003, 2004], shows that the density and organization of fractures are directly related to m; when m goes to infinity, only the largest nuclei propagates, while all fractures develop independently of their length when m is 0. If fractures are relatively independent of each others, the value K is proportional to the square root of the fracture length, so that the fracture-growth-rate equation now writes:

$$v(l) = \frac{dl}{dt} = Cl^a, \tag{4}$$

where a is the growth exponent, and C is a parameter assumed constant, which depends on the remote stress.

[21] Exponential models were based on thermodynamic theories developed for slow fracture growth in mode I [*Darot and Gueguen*, 1986; *Dove*, 1995; *Vanel et al.*, 2009]. The crack tip velocity is expected to be proportional to an exponential Arrhenius-type term, where the activation energy, G, is the energy release rate during growth. Considering the dependency of G on the fracture length l, these models predict that the fracture growth rate should increase exponentially with length:

$$v = \frac{dl}{dt} = C \exp\left(\frac{l}{l_c}\right), \tag{5}$$

where both constant C and l_c depend on temperature, stress, and elastic properties of rock materials [*Vanel et al.*, 2009]. Note that there is another exponential expression, where the fracture growth rate is proportional to the exponential function of the intensity factor K, which in turn is proportional to the square root of the fracture length l [*Dove*, 1995].

[22] Whatever the growth law, because of its fast increase with length fractures become infinite in a finite time. The so-called time to rupture t_r is characteristic of the growth law and depends on the initial nuclei length l_N: $t_r = \frac{l_N^{1-a}}{(a-1)C}$ for the power law (equation ((4)), and $t_r = \frac{l_c}{C} \exp\left(-\frac{l_N}{l_c}\right)$ for the exponential law (equation ((5)).

[23] In the next paragraph, we will discuss the fracture length distribution produced by the growth equations ((4) and ((5)).

2.3. Fracture Size Distribution for Freely Growing Fractures

[24] The fracture size distribution can be calculated from a balance between time t and $t+dt$. A fracture set $n(l,t) \times dl$ at the time t will grow to $n(l+v(l)dt, t+dt) \times dl'$ at the time $t+dt$, where dl' is the transformation of the length range dl by the fracture growth: $dl' = dl * \left(1 + \frac{dv}{dl}dt\right)$; the fracture

balance must also incorporate the set of nuclei produced during dt: $\dot{n}_N(t)p_N(l + v(l)dt) * dl' * dt$. In the limit where both dl and dt go to 0, this gives the general differential equation [see also *Sano et al.*, 1981; *Sornette and Davy*, 1991]:

$$\frac{\partial n}{\partial t} + \frac{\partial(vn)}{\partial l} = \dot{n}_N(t)p_N(l). \tag{6}$$

a) *Case where the nucleation rate $\dot{n}_N$ is constant and non-nil*

[25] This equation has a stationary solution if both $\dot{n}_N$ and $v(l)$ are time independent and non-nil:

$$n_{st}(l) = \frac{\dot{n}_N}{v(l)}(1 - P_N(l)). \tag{7}$$

with $P_N(l) = \int_l^\infty p_N(l)dl$ is the complementary cumulative probability distribution of nuclei, which is supposed to vanish rapidly. Thus, for all lengths such as $P_N(l) \ll 1$, the stationary distribution length $n_{st}(l)$ is the ratio $n_{st}(l) = \frac{\dot{n}_N}{v(l)}$, proportional to the nucleation rate by the inverse of the growth rate function. An exponentially increasing growth rate (see previous paragraph) will eventually produce an exponentially decreasing distribution length, while Charles' law is consistent with a power law:

$$n_{st}(l \gg l_N) = \frac{\dot{n}_N}{C} l^{-a}, \tag{8}$$

which is only controlled by the parameters C and a of the growth law and by the nucleation rate $\dot{n}_N$, independently of the nuclei length distribution.

[26] There is no obvious analytical solution for the nonstationary regime, but the solution may be approached by posing: $n(l,t) = \frac{\dot{n}_N}{v(l)}(\tilde{y}(l,t) + 1 - P_N(l))$, with $\tilde{y}(l,t)$ a non-stationary dimensionless term that obeys a quite simple transport equation:

$$\frac{1}{v(l)}\frac{\partial\tilde{y}}{\partial t} + \frac{\partial\tilde{y}}{\partial l} = 0. \tag{9}$$

$v(l)$, the speed term of the above equation, is increasing with l; we thus expect the stationary regime to be reached faster for large lengths than for small ones.

[27] We can also conjecture about the time scale of the process. Indeed, the above equation shows that $v(l)$ is the only function that links time and length scales. In this dynamical system, the natural length scale is the nuclei length l_N. A natural time scale would be the ratio $t_o = \frac{l_N}{v(l_N)}$, which characterizes the very first stage of nuclei growth. This time scale is of the same order of magnitude as the time to rupture t_r as defined in the previous paragraph ($t_r = \frac{t_o}{a-1}$ for the power-law equation, and $t_r = t_o\frac{l_N}{l_c}$ for the exponential function); it is likely the time to reach the stationary solution.

b) *Case where N nuclei are present at $t=0$ and no nucleation rate*

[28] If all fractures are present since beginning, the length distribution at any time t reflects the shift of the initial nuclei length distribution $p_N(l)$ by the growth rate equations ((4) and ((5). The density distribution of fracture at any time t is directly related to the initial nuclei length distribution at $t = 0$ by a one-to-one correspondence relationship:

$$n(l) \ dl = n(l_{t=0}) dl_{t=0},$$

where $l_{t=0}$ is the corresponding nuclei length. The initial density distribution $n(l_{t=0})$ is the product of the total number of nuclei N by the frequency distribution of nuclei size p_N. The fracture length $l(t)$ is obtained by integrating the growth-rate equation from its initial value: For the power-law growth model (equation ((4)), this gives:

$$l(t) = \left(l_{t=0}^{1-a} - (a-1)Ct\right)^{\frac{1}{1-a}}.$$

[29] Thus, we can derive $n(l)$ at any time t by deriving l with respect to $l_{t=0}$. We obtain the following expression for $n(l)$:

$$n(l) = N * p_N(l_{t=0}) * \left(\frac{l}{l_{t=0}}\right)^{-a}$$

$$\text{and } l_{t=0} = (l^{1-a} + (a-1)Ct)^{\frac{1}{1-a}}. \quad (10)$$

[30] As long as $l^{1-a} << (a-1)Ct$ (i.e., t is large enough), $n(l)$ is a power law, the exponent of which is minus the growth-rate exponent a:

$$n(l) = N * \frac{p_N\left(((a-1)Ct)^{\frac{1}{1-a}}\right)}{((a-1)Ct)^{-\frac{a}{1-a}}} * l^{-a}. \quad (11)$$

[31] The expression is valid for all lengths, where $p_N(l_{t=0})$ is not nil. The equation predicts (1) that the density term of the length distribution is proportional to the number of initial nuclei, and that it varies (slightly actually) with time (Figure 9a).

[32] A similar expression can be obtained for the exponential model (equation ((5)):

$$n(l) = N * p(l_{t=0}) \frac{\exp(-l/l_c)}{\exp(-l_{t=0}/l_c)}$$

$$\text{and } l_{t=0} = -l_c * \ln\left(\exp(-l/l_c) + \frac{Ct}{l_c}\right). \quad (12)$$

[33] If t is large enough $\left(t >> \frac{l_c}{C}\exp(-l/l_c)\right)$, the above equation transforms into an exponentially decreasing function, the proportionality coefficient of which decreases with time:

$$n(l) = N * p_N\left(-l_c \ln\left(\frac{Ct}{l_c}\right)\right)\frac{l_c}{Ct}\cdot\exp(-l/l_c) \quad (13)$$

c) *Which growth law is for geological fractures?*

[34] Choosing a fracture growth law consistent with geological dynamics is a tricky issue, which is beyond the aim of this paper. However, we point out that there are clearly inconsistencies between geological fracture characteristics and experimental data obtained on rock samples, or any kind of solid materials. If power laws and exponential functions have been found to adequately fit the length distributions of geological faults [*Bonnet et al.*, 2001; *Korvin*, 1989], the parameters retrieved from fault length distributions are totally inconsistent with those deduced from fracturing experimental data. The subcritical growth index of the Charles' law was found to be larger than 30 [*Atkinson*, 1984; *Ko and Kemeny*, 2011], entailing exponents a larger than 15, while the power-law length exponents a of faults are rarely larger than 4 [*Bonnet et al.*, 2001]. It is even worst for exponential fits, where atomic scale processes are invoked for experimental data [*Darot and Gueguen*, 1986], while the length scale of fault length distributions are meter to kilometer scales.

[35] These basic abovementioned arguments highlight the difficulty to upscale laboratory experiments at the crustal scale. Mechanical heterogeneities, propagation mode, and chemical processes induced or not by fluid flow are likely making the geological fracture growth law an issue. In this first paper, we choose fracture growth laws that remain consistent with measured fault length distributions. Since many analyzed length distributions are power laws [*Bonnet et al.*, 2001] (with however notable exceptions when fragmentation is likely the dominant process [*Korvin*, 1989]), we use the power-law equation (5) as a proxy for the growth of geological fracture, in the domain where it does not interact with others. An extrapolation to exponential functions can be quite easily done.

2.4. Fracture-to-Facture Interaction and Fracture Arrest

[36] As recalled in the "Introduction" section, the UFM rule imposes the arrest of fractures when they encounter larger ones. Basically, a fracture propagates until it intersects larger fractures. This rule is, however, not univocal since it makes the fracture propagation vanish beyond such fracture intersections, but it does not tell anything about the fracture growth in other directions. We define different growth/stop models according to the number of degrees of freedom of the fracture growth. The first and basic degree of freedom is the fracture radius. A fracture that uniformly grows (in directions) from a fixed center has only one degree of freedom. Its growth will be stopped as soon as it intersects
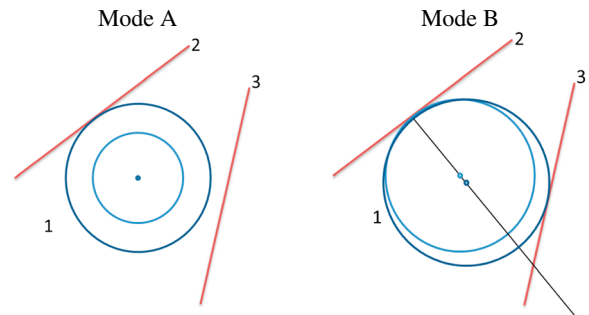

Figure 2. Illustration of the two different arrest rules. (Left) Mode A. (Right) Mode B. Fractures 2 and 3 are fixed. Fracture 1 is drawn at two different stages: light blue for the first stage where the fracture is still growing; dark blue for the second stage corresponding to the point where fracture stops growing. See text for details.

the first larger fracture. We define this as the mode-A growth model (Figure 2, mode A).

[37] An additional degree of freedom can be added by allowing the fracture center to move if necessary (Figure 2, mode B). Let us assume that the growth rate of the fracture 1 is inhibited by the intersection with a larger fracture 2. At this point, the fracture 1 is tangential to 2; it can continue to grow in all other directions as long it remains tangential to 2. This can be achieved in different ways depending on the distribution of fracture growth rate along the edge of fracture 1. If we assume that fractures remain disk-shaped (uniform growth rate along the edge), there is only 1 additional degree of freedom since the fracture center can only move along the line perpendicular to fracture 2 in order to maintain fracture 1 tangential to fracture 2. This mode is further called mode-B growth (Figure 2).

[38] Additional degrees of freedom can be added by relaxing the disk-shape hypothesis (e.g., truncated ellipses). In this paper, we only examine mode-A and mode-B growth models.

[39] For any mode of arrest, the UFM framework defined in *Davy et al.* [2010] predicts that during the growth of a fracture system, once mechanical interactions between fractures become dominant, a likely unique regime appears. It is called the UFM "dense" regime to reflect that this regime effectively defines the densest possible values of fracture size distribution.

[40] In either mode A or mode B (Figure 2), the length of the arrested fracture l is equal to twice the distance between the fracture center and the closest larger fracture plane d_P. To calculate the density distribution, we relate d_P to the average distance between fracture centers d and assume that there is a dimensionless ratio γ so that $l = \gamma d$. With this assumption, the density distribution of the dense regime is:

$$n_{\text{dense}}(l) = D\gamma^D l^{-(D+1)}, \tag{14}$$

with D the topological—either fractal or Euclidian—dimension associated to fracture centers [*Davy et al.*, 2010] that can be calculated with box-counting methods. Thus defined, γ is a geometrical number related to local spatial conditions around fractures, that is, fracture orientation distribution and also potentially fracture arrest mode.

[41] The UFM dense regime is characterized by a self-similar distribution, the length scaling exponent of which is $a_{\text{dense}} = D + 1$. The density term, $D\gamma^D$ depends only on the γ parameter, the possible variations of which are further investigated in section 4.

[42] Beyond the fracture length scaling, the UFM model leads to specific fracture-to-fracture interactions and spatial organization. The latter is reflected in the apparition of "T" fracture terminations in addition to classical "X" fracture intersections otherwise observed when fracture positions are independently assigned (like in stochastic Poissonian models).

2.5. Combination of Nucleation, Growth, and Arrest

[43] When independently considered, both the dilute (freely growing fractures) and dense (stopped fractures) regimes have stationary density limits defined by equations
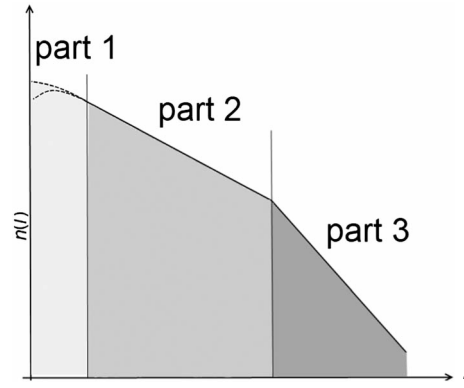

Figure 3. Illustration of the length distribution of the correlated 3D-DFN models.

((8) (or ((11)) and ((14), respectively. The three main regimes can be defined, as sketched in Figure 3: a regime partly controlled by the nuclei distribution for the smallest lengths (part 1), a regime controlled by the growth law and nuclei rate (independently of the nuclei length probability distribution) for intermediate lengths (part 2), the UFM dense regime for the largest fractures (part 3). The scale for which both stationary density distributions are equal is given by:

$$l_c = \left(\frac{D\gamma^D\, C}{\dot{n}_N} \right)^{\frac{1}{D+1-a}}. \tag{15}$$

[44] This general scheme should still be qualitatively valid when considering the three main stages of fracturing (nucleation, growth, and arrest) but with important differences. Indeed, since the total number of fractures and of fracture lengths is continuously increasing during the fracturing process (both by nucleation and fracture growth), the dense regime should spread towards smaller and smaller fractures—which is equivalent to say that arrested fractures become smaller and smaller. The combination of the stationary density equations ((8) (or ((11)) and ((14), although it is an interesting reference, cannot define the stationary regime of the whole fracturing process.

2.6. Numerical Implementation

[45] We propose a 3D time-wise DFN generation method based on the above described theoretical model. It is developed within the software platform H2OLAB [*de Dreuzy et al.*, 2010; *Erhel et al.*, 2009a, b; *Pichot et al.*, 2010]. Fractures are modeled by disks and are embedded in a 3D polyhedron.

[46] The fracture nucleation and propagation are implemented following sections 2.1 to 2.3. In practice, a virtual time t is simulated, starting from $t = 0$ to the end of the process. This time line is divided in time steps Δt; for each time step, new fractures are generated (nucleation) and fracture propagation is applied.

[47] At each time step, $\dot{n}_N \Delta t$ nuclei are generated. These nuclei are created at a time that is uniformly spread within the time step, in order to better reproduce a continuous nucleation.

[48] Fracture length is increased according to equation ((4), which yields:

$$l(t + \Delta t) = \left(l(t)^{1-a} + (1-a) \cdot C \cdot \Delta t\right)^{\frac{1}{1-a}}. \qquad (16)$$

[49] The generation scheme is sketched below:

---

    1) Initialization: $t := 0$

Then the dynamic process starts. It is composed as follow:

    2) Set $t := t + \Delta t$

    3) Nucleation stage:

        ○ define new nuclei

        ○ keep new nuclei only if no intersection with existing fractures,

    4) Fracture growth stage - Eq. (16)

    5) Computation of intersections

    6) Fracture-length reduction according to mode A or mode B

    7) Check ending criteria

        ○ If criteria are fulfilled, go to step 8),

        ○ else, return to step 2).

Finally, the generation is stopped:

    8) Finalization, computation of intersections and statistics on the DFN.

---

[50] Note that the nuclei are not added in the system if they are arrested by the existing fracture network. The effective nucleation rate is, thus, likely decreasing with time as the space available for new nuclei is decreasing. This point will be discussed in the next paragraphs.

[51] During one time step, a fracture may grow so that it intersects more than one (in mode A) or two (in mode B) fractures. In such case, the intersected fractures are sorted according to their respective distance to the growing fractures and the arrest rule accordingly applied. The time step is reduced to minimize such conflicts.

[52] In practice, the DFN is generated in a cubic volume of side L. Nucleation occurs only in the cube. Borders of the generation cube act as limits, beyond such fractures are not allowed to grow. No edge effects have been detected with these rules mainly because the total surface of fractures is rapidly much larger than the boundary surfaces, and the contribution of the latter to stopping internal fractures becomes negligible.

[53] In principle, the DFN can grow until there is no more available space to put new nuclei or to propagate one fracture. Some ending criteria are defined:

[54] 1. Nucleation is stopped when no nuclei can be added in the system, and no fracture can grow anymore;

[55] 2. Nucleation is stopped after a while, so as to obtain a fixed length distribution;

[56] 3. Nucleation is stopped when the targeted fracture density is achieved.

3. Numerical Simulations of the DFN Model

[57] The model described in the previous paragraph is defined by a set of assumptions (Table 1) and parameters: $p(l)$, $\dot{n}_N(t)$ for nucleation; C, a for the growth law; mode A or B for the arrest condition. Length, density distribution, and time are given in an dimensionless form by normalizing with the characteristic length l_o and/or the characteristic time t_o: $t' = t/t_0$, $l' = l/l_0$, $n'(l') = n(l) * l_0$, $p_N'(l') = p_N(l) * l_0$, and

$\dot{n}_N'(t') = \dot{n}_N(t) * t_o$. The characteristic length scale l_o is the nuclei length $l_o = l_N$, and the time scale t_o is $t_o = \frac{l_N}{v(l_N)} = \frac{1}{C l_N^{a-1}}$, which is close to the time to rupture for nuclei of size l_N.

3.1. Freely Growing Fracture Distribution

[58] The numerical model is first used to check the stationary density regime of the free growth regime and to calculate non-stationary stages of the fracture growth phase. Figure 4 illustrates the different density distributions obtained at dimensionless times of 0.1 to 5 with model parameters given in the figure legend. The stationary solution of the growth process (equation ((7)) is reached at t' close to 0.5, the time necessary for a fracture of initial length l_N to grow to infinity. At this point, the amount of new fractures compensates the fracture propagation and the final length density distribution tends to the expected power law (equation ((8)), with a scale exponent a (i.e., the growth exponent) and a density term α equal to the ratio between nucleation rate $\dot{n}_N$ and growth coefficient C.

[59] The variations in the density distribution, observed at large length ($l' \geq 50$), simply reflect the small number of large fractures. In the example, only 30 fractures are larger than $l' = 50$, 1400 than $l' = 10$, and 6×10^5 larger than $l' = 1$ (i.e., the smallest nuclei).

3.2. Density Distribution of the Complete Fracturing Model with Nucleation, Growth, and Arrest

[60] Now, all the stages of the fracturing process are considered to yield DFN, the statistical characteristics of which

Table 1. Summary of the Model Assumptions

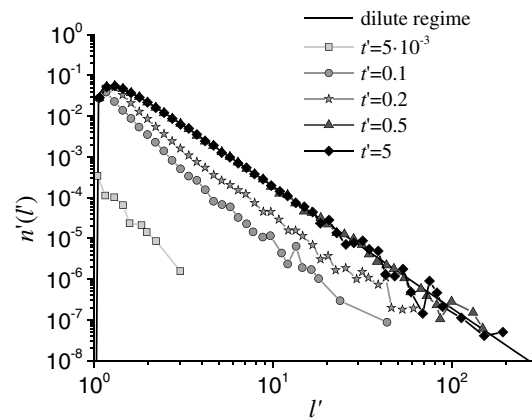|	Features
Nucleation	−Spatial Distribution: Uniform
	−Orientation Distribution: Uniform, One Set, or Three Sets
	−Length Distribution: Power Law or Exponential
	−Nucleation Rate: Constant or All Nuclei Present at $t = 0$
Growth	Power Law Equation
Fracture Arrest	Mode A or Mode B

Figure 4. Evolution with time of the length distribution of the freely growing model without arrest. The parameters for the simulations are a power-law nuclei distribution $p_N(l)$ with $b = 5$ and $l_N = 10^{-2}$, a nucleation rate $\dot{n}_N = 19$, a growth law with $C = 1$ and $a = 3$, and a system size $L = 1$.

are analyzed. The numerical parameters of the growth process are the ones used in the previous section (Figure 4). The numerical model covers more than two orders of magnitude of fracture length, from l' equal to 1 to the dimensionless system L' size equal to 100. The growth parameters are chosen such that the critical transition dimensionless transition scale $l'_c = l_c/l_0$ (equation ((15)) is close to 10. We, thus, expect both the dilute and dense regimes to be observed within this range of length scales. The arrest rule is applied in mode A (section 2.4). Plots of several stages of the DFN distribution are displayed in Figure 5. Corresponding 2D trace map views (defined by 2D cutting of the 3D DFN) of the generated DFN are provided in Figure 8.

[61] At the earliest stages of the generation, most of the fractures still belong to the nuclei distribution ($t' = 5 \times 10^{-3}$). The density distribution is comparable to the free-growth model (see Figure 5a) up to $t' = 0.1$, although all fractures larger than 10 are already arrested (Figure 5b). The UFM dense regime is well defined in the density distribution from $t' = 0.1$.

[62] At t' about equal to 0.5, the density distribution is a combination of both the stationary regime of the free-growth (dilute) regime (for $l' < l'_c$) and the dense UFM regime ($l' > l'_c$). l'_c, the transition scale between both regimes, is as defined as in equation ((15)). All fractures larger than l'_c (=10) are arrested, as well as a significant part of smaller fractures.

[63] For time t' larger than 0.5, the UFM regime spreads over a very large range of fracture scales. It is only limited at small scale by the nuclei distribution. Except the smallest fractures, no or few fractures are anymore growing ($t' = 5$ in Figure 5).

[64] At any time, the UFM regime corresponds to an upper density limit of the eventual distribution. In this example, the UFM dense regime (equation ((14), red dashed line in Figure 5a) can be clearly identified for $t' \geq 0.5$, with an estimated density term ($D\gamma^D$ in equation ((14))) equal to 2.1. Figure 6 shows the lower limit l_t of the UFM regime defined from visual observation of the density distribution. l_t exhibits a fast exponential decrease for time smaller than 0.25 down to l_c; after, the decrease continues but much slower. The produced DFN is, therefore, in the dense regime above l_t and in a mixed regime (partly dense, partly dilute) below l_t.

[65] To illustrate the evolution of the bulk fracture density, we then calculate the mass density d_m, which is the total surface of fractures produced within the system:

$$d_m = \int_{l_0}^{L} n(l) \frac{\pi l^2}{4} dl, \qquad (17)$$

[66] Figure 7a shows that the dimensionless density $d'_m = d_m \cdot l_0$ follows the same evolution regimes as l_t: it increases fast up to time $t' = 0.5$ and thereafter continues to increase but at much smaller rates. The effective nucleation rate (Figure 7b), which do not take account of nuclei intersecting pre-existing fractures, is decreasing in this modeling as the available space for nucleation V_N is decreasing with time. V_N can be estimated as $V_N = V_{Total} - d_m \times l_N$, where $d_m \times l_N$ is the volume around the pre-existing fracture network that is not available for further nuclei. Figure 7b shows that the nucleation rate decreases as V_N for time $t' \leq 1$ and slightly slower thereafter. The slight discrepancy may be due to the simplistic formula used to define V_N that does not take account of fracture overlapping.

[67] Figure 8 shows 2D trace maps derived from the 3D fracture networks at different times. At the early stages, the network is characterized by a few large fractures that grow fast after nucleation, surrounded by small nuclei that have not yet grown. These large fractures act as barriers for later fracture development, and the network density then increases in between the arrested fractures. In 3D, there are only a few X-type fracture intersections and a large number
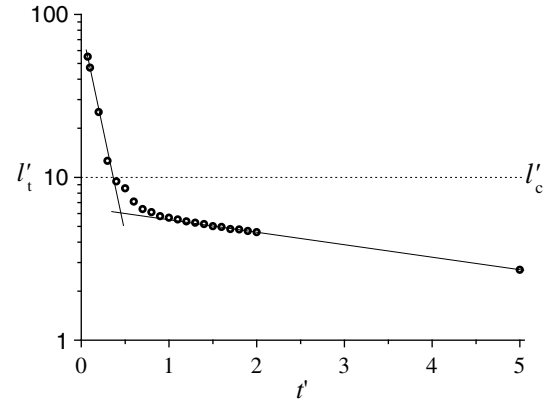

Figure 6. Evolution of the limit of the UFM regime (i.e., the smaller fracture length l_t that follows the UFM distribution) with dimensionless time t'.
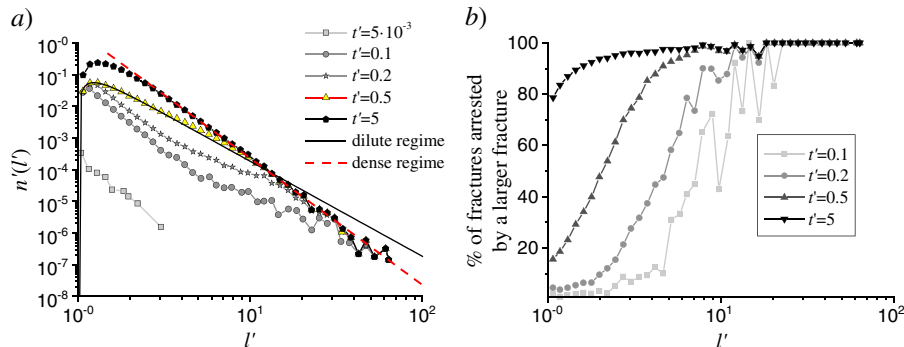

Figure 5. (a) Evolution with time of the length distribution with mode A and other parameters same as in Figure 4. (b) Percentage of arrested fractures.
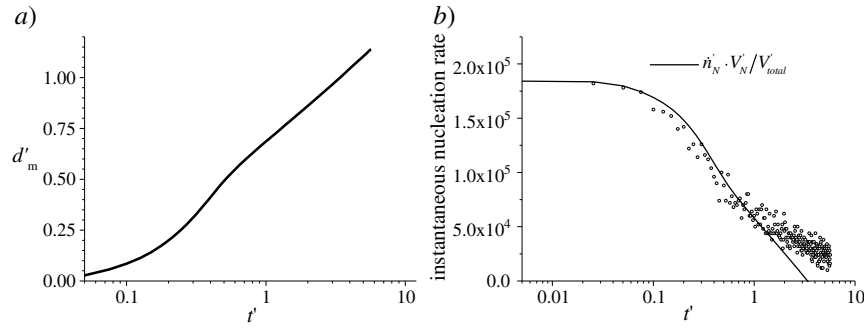
Figure 7. Evolution of (a) network density and (b) instantaneous nucleation rate with dimensionless time t'.
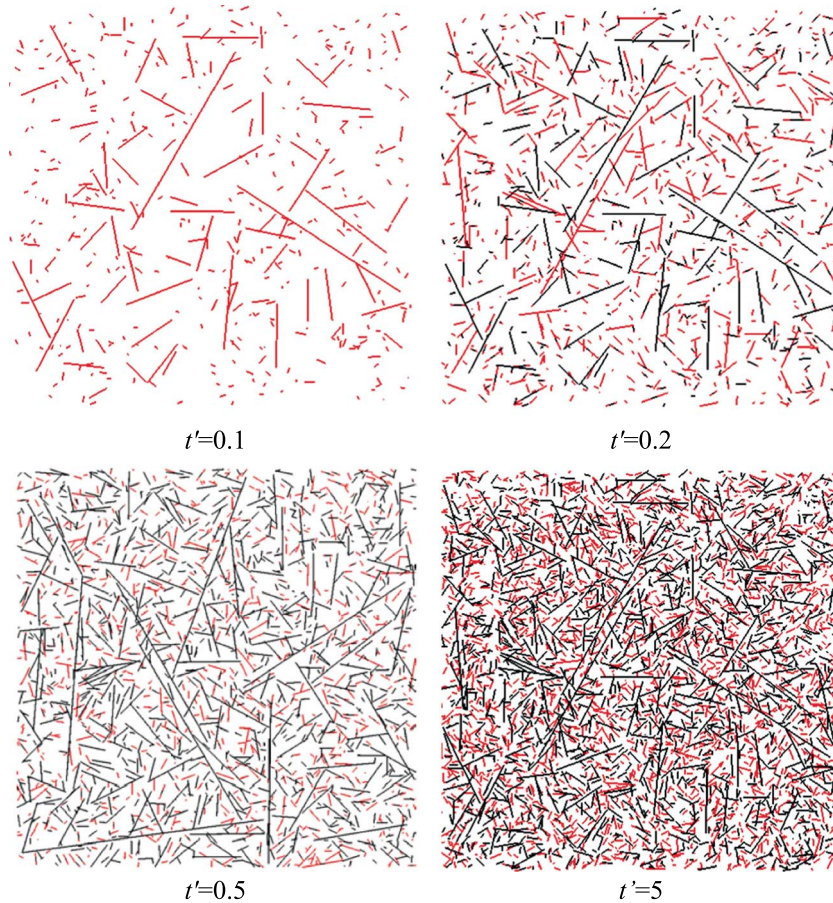

$t'=0.1$

$t'=0.2$

$t'=0.5$

$t'=5$

Figure 8. Illustration of the DFN generation and evolution (same as Figure 5). 2D trace map views—(xy) plane, $z=0$—from a 3D DFN generation with the following parameters: a power-law nuclei distribution with $b=5$ and $l_N=10^{-2}$, a nucleation rate $\dot{n}_N = 19$, a growth law with $C=1$ and $a=3$, and a system size of length $L=1$. The fractures generated between the previous and the current time steps are displayed in red.

of T-intersections. Note that in 2D, because of stereological effects (observing a 3D structure from a 2D map), fractures may seem to be disconnected (in Figure 8 for instance), while they are actually not in 3D (as quantified in Figure 5b for instance). This is a difficulty when attempting to demonstrate the UFM organization from outcrops.

[68] The case where all nuclei are initially present with no nucleation rate has also been investigated (Figure 9). The density distribution of freely-growing fractures (Figure 9a) is well described by the equations ((10) and ((11): the length distribution eventually stabilizes into a power law, the exponent of which is $-a$ with a the growth-law exponent; the density term is slightly increasing with time as well as the lower bound of the distribution, emphasizing the continuous length increase of nuclei. With UFM arrest rule, here in mode A (Figure 9b), the behavior is very similar to the case where nuclei are progressively created. The density distribution shows both regimes: the free-growth model for small lengths, and the UFM regime for large lengths. The transition length l_c' is decreasing with time, emphasizing the spreading of the
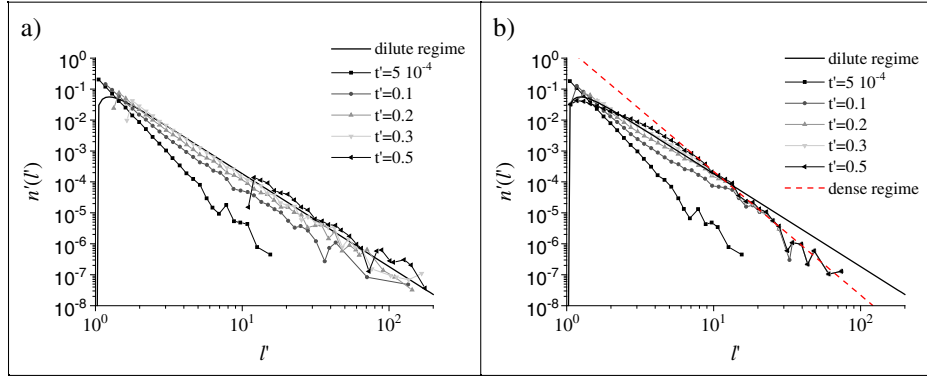
Figure 9. Evolution with time of the length distribution with no nucleation rate. All the 65,571 nuclei are present at the simulation start; this number is the same as in the case with nucleation rate for $t' = 0.5$ (Figure 5). Other parameters are the same as in Figure 5. (a) Model with no arrest conditions (freely growing fractures). (b) Model with mode A arrest rule.

UFM regime towards small lengths. The equation of the UFM regime is exactly similar to the one obtained for the nucleation-rate case.

[69] The results presented in this paragraph have been obtained with a power-law nuclei length distribution. The results are similar for other types of nuclei length distribution except in the range of lengths that overlap the initial nuclei distribution lengths.

4. The Dimensionless Density of the UFM Mode

[70] The density term of the UFM mode d_{UFM} is a dimensionless parameter that is still to be assessed (see equation ((14)). *Davy et al.* [2010] postulates that d_{UFM} depends only on the network dimension D and on the ratio γ between the fracture length and the distance to intersecting fracture: $d_{UFM} = D\gamma^D$. Considering this definition, γ and thus d_{UFM} are thought to depend mainly on both parameters. The fracture orientation and the fracture arrest mode. In the present section, we investigate the possible variations of d_{UFM}.

[71] Since d_{UFM} defines the static stationary regime for dense networks, it is not likely dependent on the way this regime is reached, and thus on any nucleation and growth-law parameters. We indeed verify that d_{UFM} is independent of the parameters C, a, $\dot{n}_N$, and $p_N(l)$.

[72] By definition, d_{UFM} describes the relationship between the fracture length and the fracture density. This parameter is potentially dependent on the details of the arrest rule and on fracture orientations, which both affect fracture intersections and thus the ratio between arrested fracture length and the distance to larger fractures. Both aspects are reviewed below.

4.1. d_{UFM} and the Mode of Fracture Arrest

[73] The generation mode (mode A and mode B, see section 2.4) influences the possible length that a fracture can reach before being arrested. In mode A, a fracture stops after the first intersection with a larger fracture; in mode B, it can grow further until it crosses a second larger one, entailing densities larger than those in mode A. This is illustrated in Figure 10, where two DFN models with uniform orientations, only differing in their arrest mode, lead to slightly different UFM dense regimes. As expected, the scaling length exponent
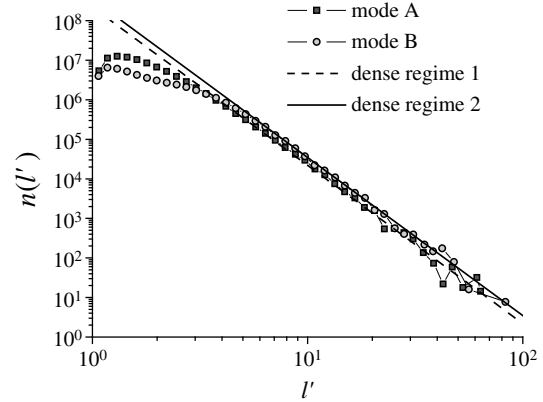

Figure 10. Length distribution for mode A and mode B UFM. Generation parameters are similar to Figure 5 and final mass density $d'_m = d_m \cdot l_0$ qual to 0.9.

of the UFM regime is identical for both modes; only the density term is different, equal to 2.1 and 3.0 in modes A and B, respectively.

4.2. d_{UFM} and the Orientation Distribution

[74] The density term d_{UFM} is dependent on the probability of fracture intersection, which itself is known to be strongly dependent on the fracture orientation distribution [*Balberg et al.*, 1984]. At the extreme, if fractures are all perfectly parallel, no intersection is possible and large lengths are not inconsistent with large densities, entailing large values for d_{UFM}.

[75] In order to assess the link between fracture orientation distribution and the density term of the UFM regime, we consider fracture sets, the pole orientation of which varies in both dip and strike by an angle θ. Formally, the dip and strike orientation distribution of nuclei are defined by a Gaussian distribution centered on the average with a standard deviation $\sigma_\theta = \theta$.

[76] We then consider two orientation models: (i) a one-set model, where fractures are strictly parallel if $\theta = 0$, and subparallel if θ is greater than 0 (see an example of 2D trace map in Figure 11a), and (ii) a three-set model constituted of three fracture sets, the average orientation poles of which are perpendicular (Figure 11b).
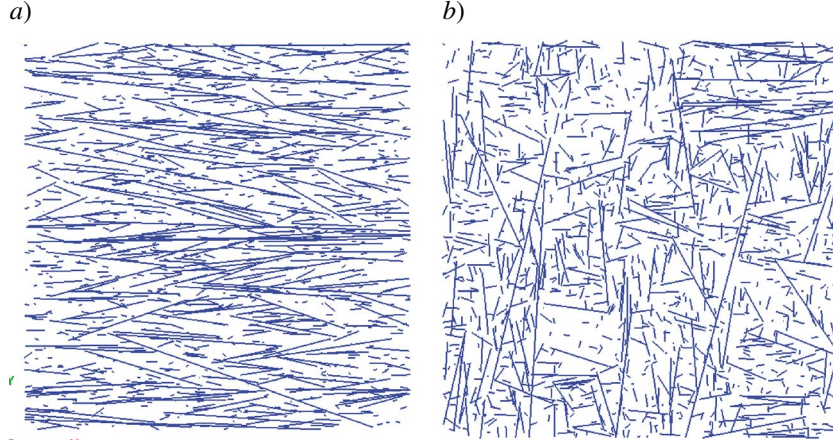
a)   *b)*

Figure 11. 2D trace map views of 3D DFNs with (a) one single set and (b) three orthogonal fracture sets.

[77] Intensive simulations are performed to assess numerically the density term d_{UFM} ($=D\gamma^D$) of the UFM distribution and its relation to fracture orientations. In each case, the DFN generation is stopped when a constant mass density is reached, and final density terms are averaged over 20 realizations (the statistical variability is less than 6%). The one-set and three-set cases, with $\theta = 15°$, are displayed in Figure 12. It shows that the final density term is larger for the one-set model than for the three-set orthogonal model.

[78] Table 2 and Figure 13 summarize the values of d_{UFM} associated to the various types of pole orientation distributions (uniform in the range 0–360°, one set, and three orthogonal set) both in mode A and mode B.

[79] Depending on the anisotropy and arrest mode, the density term varies from 2.0 up to 32. Whatever the orientation distribution, the density term in mode B is larger than that in mode A by 50% (factor close to 1.5). For the one-set case, the density term is found to vary with θ as:

$$d_{\mathrm{UFM}} = \frac{2}{\sin(\theta)} \text{ for mode } A, \quad d_{\mathrm{UFM}} = \frac{3}{\sin(\theta)} \text{ for mode } B \quad (18)$$

[80] The $\sin^{-1}$ correction conveys the geometrical correction between the fracture length necessary to intersect another fracture and the distance between fracture centers.

[81] For the three-set perpendicular model, the density term is about constant for θ larger than 15°. For smaller θ, it slightly increases by a factor of 1.5 (mode A) or 2.5 (mode B). In this case where the sets are orthogonal, fractures are easily intersecting a fracture from one of the two other sets, and the distance between intersecting fractures is about insensitive to θ.

5. Discussion

[82] The model presented in this paper is basically a versatile way to generate fracture systems; it is much simpler and faster than models based on complete fracture mechanics. It enables to produce geometries with the same length-density scaling as natural fracture networks. Based on initially uniformly distributed nuclei, the combination between fracture growth and arrest finally yields complex networks with spatial correlations involving fracture tips, position,

Table 2. Values of $D\gamma^D$ for Varying Fracture Pole Orientation Distributions, Both in Mode A Mode B

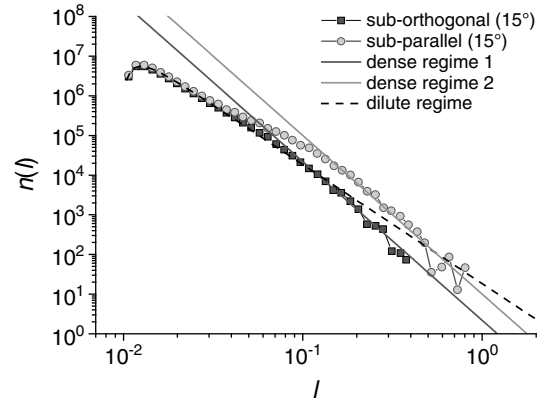| Pole Orientations	Variability	d_{UFM} in Mode A	d_{UFM} in Mode B
One Set	5	22	33
	15	7.2	11.8
	30	3.6	6.3
	45	2.5	5.1
Three Orthogonal Sets	1	3.1	7.5
	5	2.4	5
	15	2	3.7
	30	2	3.1
	45	2	3.0
Uniform		2	3.0

Figure 12. DFN pole orientation distribution influence on the DFN structure and UFM dense density term.

orientation and size, together with power-law size distributions where the exponents of which are controlled either by the free growth rate or by interactions between fractures. Such characteristics are much more realistic than otherwise widely used random (Poissonian) DFN models, where fracture geometrical characteristics are independently stated and randomly generated, leading to a lack of spatial correlations.

[83] The model does not encounter the typical computation limitations due to the complexity inherent to resolution
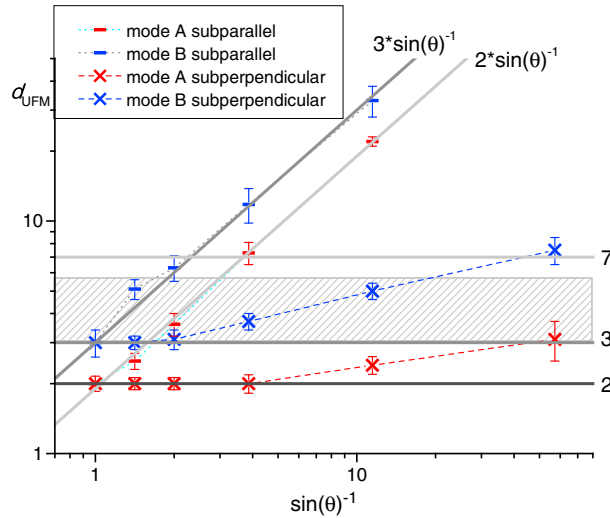
Figure 13. Evolution of the UFM density dUFM as a function of the angular variability θ (see text).

of fully mechanical approaches; on the reverse, its capacity to reproduce real properties of natural fracture systems is possibly limited by an oversimplification of mechanical rules. We review below the potential limitations.

[84] There is no explicit rule to stop fracture generation. Currently, the DFN density continues increasing until there is no more space for fractures to nucleate (from the minimum size l_N) or grow. However, we do observe that the density increases rapidly up to dimensionless time of 0.5, i.e., the time necessary for the smallest nuclei to reach the largest scale. Thereafter the fracture density increase is much slower. The specific point $t' \sim 0.5$ is thus close to a quasi-stationary regime; at this point, the fracture length distribution is defined at small length by the free-growth (dilute) regime (i.e., the stationary length distribution eventually yielded by the fracture growth law), and at large lengths by the UFM (dense) regime. After $t' = 0.5$, the DFN growth is much slower than before, since it becomes more and more difficult to add active nuclei in the system. Finally, the fracture network stops growing when the distance between fractures is as small as the characteristic nuclei length scale l_N. Adding energy considerations on the fracturing process would be a possible improvement to the model. In quasi-static fracturing process (neglecting heat dissipation, wave radiation, and plastic deformation), the potential energy is partitioned into elastic deformation and creation of new fracture planes [*Griffith*, 1920]. It is thus likely increasing with fracture density and growth. Studying this energy increase could be useful for determining the eventual final stage of the fracturing process. Although this issue is beyond a simple DFN model, it could be useful to find the rule-of-thumb reasons that determine when the fracturing process stops.

[85] The second limitation is relative to nucleation (nuclei are viewed as "activated" flaws, i.e., potentially growing). Currently, the model nucleation is uniformly distributed through space. In reality, nucleation is more likely locally conditioned by local stress field variations, especially increased in the vicinity of the tips of previous fractures. Since the UFM regime is defined by fractures large enough to intersect each others, we do not expect a significant consequence

on the model size distribution. However, beyond a certain level, local stresses may limit the nucleation itself and yield a natural final stage of the fracture system growth as immature as those observed for small time evolution (for instance $t' = 0.2$ in Figure 5a, which is not far from what is observed for the San Andreas fault system). In a further work, we aim to study this process in the same spirit as random-fuse models [*Hansen et al.*, 1991; *Zapperi and Nukala*, 2006].

[86] A similar reasoning can be applied to the growth rate formulation, which is likely proportional to the stress intensity factor K. This entails a dependency of orientation and growth rate on the local stress field. The calculation of the local stress field would dramatically reduce the model performance and thus its capacity to simulate complex networks, but simple rules can be sought to account either for the orientation of the remote stress field (case of isolated fracture growth) or for the vicinity of larger fractures in a simplified stochastic way. Note, however, that this improvement requires knowing the tectonic (or body) stress field that occurred during the fracture network growth.

[87] An additional improvement of the model can be done by considering different stages of the tectonic history if it is observed that the different fracture families form as a sequence in time. This sequential nucleation or growth can be easily introduced in this modeling framework.

[88] Finally, the fracture disc-shape assumption, which may be reasonable when fractures are isolated and only growing with respect to far field stress (isotropic growth), deserves to be improved when fractures are going to be arrested by others and then may be subjected to anisotropic growth. Furthermore, fracture shape, arrest configuration, and fracture intersection sizes are closely related. The interplay between these three elements may also have an indirect effect on the fracture density term d_{UFM}.

[89] In the proposed model, a fracture is stopped tangent to a blocking fracture, so that the intersection between both is just a point. In nature, intersections can be larger and form channels or zones of weakness with consequences on rock strength and permeability [*Abelin et al.*, 1991]. To our knowledge, no observations or data analyses are available to better constrain fracture intersection sizes in 3D. Further work is required to learn more about the length distribution of fracture intersections, for instance from a stereological analysis of intersection patterns observed on detailed 2D outcrop trace maps. If the fracture intersection is allowed to be larger than a single point, this will entail a systematic increase of fracture radius in the UFM regime, and thus an increase of the fracture density term d_{UFM}. This effect can be evaluated as follows: according to equation ((14), an increase of all fracture lengths by a coefficient ε ($l' = (1 + \varepsilon)l$) will increase the distribution density by $(1 + \varepsilon)^{a-1} - 1$ or $(a-1)\varepsilon$ if $\varepsilon << 1$. Since $a = 4$ in the UFM regime, the density increases is three times the average length increase, which may be not negligible. Note that the H2OLAB software platform, with which the present numerical modeling is developed, describes fractures as truncated ellipses. Dealing with large intersections can thus be easily implemented.

[90] Despite the above mentioned limitations, the proposed DFN model naturally produces, from very few rules, the widely observed power-law and even self-similar, density distributions of natural fracture systems. The obtained density is consistent with fracture network measurements. *Davy et al.*

[2010] has shown that the scaling and density of the UFM model is consistent with different kinds of fracture systems: joint and fault systems in different places of Norway (Hornelen basin [*Bour et al.*, 2002; *Odling*, 1997]), of Sweden (Forsmark, Simpevarp, and Laxemar [*Darcel et al.*, 2004; *Darcel et al.*, 2009; *Fox et al.*, 2007; *La Pointe et al.*, 2008; *SKB*, 2004b; *Stephens et al.*, 2008; *Wahlgren et al.*, 2008]), and of the San Andreas fault system [*Bour and Davy*, 1999; *Davy*, 1993]. Most of the observations on natural fracture systems were made from 2D outcrop mapping, for which the density terms of the length density distribution was calculated [*Davy et al.*, 2010]. For Sweden and Norway joint systems, the UFM regime is well defined above 3–5 m, with the expected 2D power-law length exponent of 3 and an apparent 2D density term varying between 2.2 to 4.5. The 3D-equivalent density, calculated by applying stereological rules [*Davy et al.*, 2006b; *Piggott*, 1997], has been found to vary between 3 and 5.5 (indicated by a grey-shaded rectangle in Figure 13 of *Davy et al.* [2010]) for the Simpevarp [*Darcel et al.*, 2004] and Forsmark sites [*Darcel et al.*, 2006]. This range is consistent with both arrest modes A and B, as long as the orientation variability (equivalent to θ in the previous paragraph) is larger than 20°–30°. Such range of orientation anisotropy is currently observed on borehole logs and outcrop maps. No similar 3D analysis has yet been performed for the Hornelen basin and San Andreas fault system. A more thorough analysis will require a complete stereological analysis for each borehole log and outcrop map. This is beyond the scope of the present study. This work is, however, starting as part of continuing investigations conducted by the SKB Company at the Äspö HRL and Forsmark sites.

[91] Because of its particular spatial correlations and intersection properties, the application of the present framework to flow and mechanical modeling may end up in new relations between DFN geometrical properties (density, scale) and consecutive flow or mechanical properties. This is likely to have consequences on flow as illustrated in the very first calculations presented in *Davy et al.* [2010]. Another geometrical characteristic of the DFN produced with this model is that the transition length l_c between the dilute and dense/UFM regimes is actually a characteristic block size for unfractured domains. Fractures smaller than l_c are poorly connected, and thus hardly define blocks in 3D. In the UFM regime (fracture length larger than l_c), fractures form an interconnected network, the distance of which between fractures is about l_c. This block size is a critical parameter for any mechanical study of rock mass (see for instance [*Hoek and Brown*, 1997]).

[92] The promising capacity of the UFM model to reflect geometrical observations finally reinforces the potential of this model to be also relevant for modeling flow and mechanical applications of natural systems. Moreover, the UFM length distribution, the scaling properties of which are fully defined, fixes an upper limit of any fracture size distribution model that cannot be bypassed. Such characteristic strongly reduces uncertainty in the DFN modeling.

6. Conclusion

[93] In this paper, we aim to improve stochastic DFN models by developing a method which reproduces the main stages of fracture evolution while preserving the currently observed scaling characteristics. The model combines, in a time-wise process, a spatially uniform nucleation of fractures, a power-law model of fracture growth and a growth arrest rule when fracture intersects another larger one. The latter aspect was firstly described in *Davy et al.* [2010]. Thus defined, the generation process naturally creates internal spatial correlations, together with multiscale fracture size distributions, producing statistical properties that are equivalent to those of real fracture systems.

[94] The statistical properties of produced DFNs were analyzed by calculating the density distribution of fracture length $n(l)$, which describes the relationship between fracture length and density. $n(l)$ can be divided in three regions: for small lengths, it is mainly controlled by the size distribution of nuclei; for intermediate lengths, it depends on both the fracture growth law and nucleation rate, converging to a well-defined power law with a scaling exponent equal to minus the growth rate exponent. At large lengths, $n(l)$ converges to the self-similar UFM regime defined in *Davy et al.* [2010], where the scaling exponent is $-(D+1)$, with D the (possibly fractal) topological dimension of the network centres. The dimensionless density term, d_{UFM}, is a function of the fracture (thus nuclei) orientation distribution, and of the details of the arrest rule.

[95] The relative importance of the three above-mentioned regimes evolves throughout the generation process. At earliest times, most of the fractures belong to the initial nuclei size distribution. The total fracture mass (i.e., sum of fracture areas) is growing at constant rate up to the time necessary for the smallest nuclei to reach the largest scale. At this intermediate stage, for which no fracture can grow freely anymore, $n(l)$ follows both the stationary free-growing regime and the dense/UFM, respectively, below and above a transition scale. After that time, if more nuclei are activated, the fracture mass goes on increasing (but at a much slower rate), and the UFM/dense regime tends to spread toward smaller and smaller fracture lengths.

[96] The UFM/dense regime is the most striking feature of produced DFN. While fractures are growing, it spreads out from the largest length (about the system size) to smaller and smaller lengths. The scaling exponent is uniquely defined, but the density term depends on the mode of arrest (factor 2/3 between mode A and mode B) and on the eventual fracture orientation distribution. The UFM density distribution is in good accordance with several field cases (especially for the Laxemar and Forsmark sites in Sweden and Hornelen basin in Norway). Finally, this model strongly reduces uncertainties inherent to any DFN modeling exercise. The UFM regime is also an upper limit of any fracture length distribution where T-intersections prevail (which seems to be the general rule in fracture systems). This brings an interesting constrain to any DFN modeling.

[97] Improving DFN modeling is of primary importance to improve flow and mechanical modeling of underground systems, especially in a context where data are very scarce with regard to the fracture network complexity. Identifying some basic rules of fracture organization as we do in this paper is an interesting way to come closer to geological complexity. The good adequacy of the UFM model with simplified mechanical rules and with field data observations reinforces the potential of this model to be also relevant for the application to flow and mechanical modeling of natural fractured systems.

References

Abelin, H., L. Birgersson, L. Moreno, H. Widén, T. Ågren, and I. Neretnieks (1991), A large-scale flow and tracer experiment in granite: 2. Results and interpretation, *Water Resour. Res.*, 27(12), 3119–3135, doi:10.1029/91wr01404.

Ackermann, R. V., and R. W. Schlische (1997), Anticlustering of small normal faults around larger faults, *Geology*, 25(12), 1127–1130, doi:10.1130/0091-7613(1997)025<1127:aosnfa>2.3.co;2.

Alava, M. J., P. K. V. V. Nukala, and S. Zapperi (2006), Statistical models of fracture, *Adv. Phys.*, 55(3-4), 349–476, doi:10.1080/00018730300741518.

Ashby, M. F., and C. G. Sammis (1990), The damage mechanics of brittle solids in compression, *Pure Appl. Geophys.*, 133(3), 489–521, doi:10.1007/bf00878002.

Atkinson, B., and P. Meredith (1987), The theory of subcritical crack growth with applications to minerals and rocks, in *Fracture Mechanics of Rock*, edited by B. K. Atkinson, pp. 111–166, Academic Press, London, Orlando.

Atkinson, B. K., and P. G. Meredith (1981), Stress corrosion cracking of quartz: A note on the influence of chemical environment, *Tectonophysics*, 77(1–2), T1–T11, doi:10.1016/0040-1951(81)90157-8.

Atkinson, B. K. (1982), Subcritical crack propagation in rocks: Theory, experimental results and applications, *J. Struct. Geol.*, 4(1), 41–56, doi:10.1016/0191-8141(82)90005-0.

Atkinson, B. K. (1984), Subcritical crack growth in geological materials, *J. Geophys. Res.*, 89(B6), 4077–4114, doi:10.1029/JB089iB06p04077.

Atkinson, B. K. (1987), *Fracture Mechanics of Rock*, 534 p., Academic Press, London, Orlando.

Balberg, I. C., H. Anderson, S. Alexander, and N. Wagner (1984), Excluded volume and its relation to the onset of percolation, *Phys. Rev. B*, 30(7), 3933–3943.

Berkowitz, B., O. Bour, P. Davy, and N. Odling (2000a), Scaling of fracture connectivity in geological formations, *Geophys. Res. Lett.*, 27(14), 2061–2064, doi:10.1029/1999GL011241.

Berkowitz, B., H. Scher, and S. Silliman (2000b), Anomalous transport in laboratory-scale, heterogeneous porous media, *Water Resour. Res.*, 36(1), 149–158.

Betekhtin, V., and A. Kadomtsev (2005), Evolution of microscopic cracks and pores in solids under loading, *Phys. Solid State*, 47(5), 825–831, doi:10.1134/1.1924839.

Bonnet, E., et al. (2001), Scaling of fracture systems in geological media, *Rev. Geophys.*, 39(3), 347–383, doi:10.1029/1999rg000074.

Bour, O., and P. Davy (1997), Connectivity of random fault networks following a power law fault length distribution, *Water Resour. Res.*, 33(7), 1567–1583, doi:10.1029/96wr00433.

Bour, O., and P. Davy (1998), On the connectivity of three-dimensional fault networks, *Water Resour. Res.*, 34(10), 2611–2622, doi:10.1029/98wr01861.

Bour, O., and P. Davy (1999), Clustering and size distributions of fault patterns: Theory and measurements, *Geophys. Res. Lett.*, 26(13), 2001–2004, doi:10.1029/1999GL900419.

Bour, O., P. Davy, C. Darcel, and N. Odling (2002), A statistical scaling model for fracture network geometry, with validation on a multiscale mapping of a joint network (Hornelen Basin, Norway), *J. Geophys. Res.*, 107(B6), ETG 4-1–ETG 4-12, doi:10.1029/2001JB000176.

Bourne, S. J., and E. J. M. Willemse (2001), Elastic stress control on the pattern of tensile fracturing around a small fault network at Nash Point, UK, *J. Struct. Geol.*, 23(11), 1753–1770.

Buchel, A., and J. P. Sethna (1997), Statistical mechanics of cracks: Fluctuations, breakdown, and asymptotics of elastic theory, *Phys. Rev. E*, 55(6), 7669.

Caumon, G., P. Collon-Drouaillet, C. L. de Veslud, S. Viseur, and J. Sausse (2009), Surface-based 3D modeling of geological structures, *Math. Geosci.*, 41(8), 927–945, doi:10.1007/s11004-009-9244-2.

Charles, R. (1958), Dynamic fatigue of glass, *J. Appl. Phys.*, 29(12), 1657–1662.

Cowie, P. A., and C. H. Scholz (1992a), Physical explanation for the displacement-length relationship of faults using a post-yield fracture mechanics model, *J. Struct. Geol.*, 14(10), 1133–1148.

Cowie, P. A., and C. H. Scholz (1992b), Growth of faults by accumulation of seismic slip, *J. Geophys. Res.*, 97(B7), 11085–11095.

Cowie, P. A., C. Vanneste, and D. Sornette (1993), Statistical Physics Model for the spatiotemporal evolution of faults, *J. Geophys. Res.*, 98(B12), 809–821.

Cowie, P. A., D. Sornette, and C. Vanneste (1995), Multifractal scaling properties of a growing fault population, *Geophys. Int. J.*, 122, 457–469.

Crampin, S. (1994), The fracture criticality of crustal rocks, *Geophys. J. Int.*, 118(2), 428–438.

Crampin, S. (1999), Implications of rock criticality for reservoir characterization, *J. Pet. Sci. Eng.*, 24(1), 29–48.

Darcel, C., O. Bour, and P. Davy (2003a), Stereological analysis of fractal fracture networks, *J. Geophys. Res.*, 108(B9), doi:10.1029/2002JB002091.

Darcel, C., O. Bour, P. Davy, and J. R. d. Dreuzy (2003b), Connectivity properties of two-dimensional fracture networks with stochastic fractal correlation, *Water Resour. Res.*, 39(10), SBH 1-1–SBH 1-13, doi:10.1029/2002wr001628.

Darcel, C., P. Davy, O. Bour, and J. R. de Dreuzy (2004), *Alternative DFN Model Based on Initial Site Investigations at Simpevarp*, 107 pp., Svensk Kärnbränslehantering AB.

Darcel, C., P. Davy, O. Bour, and J. De Dreuzy (2006), Discrete Fracture Network for the Forsmark Site, 94 pp., Svensk Kärnbränslehantering AB.

Darcel, C., P. Davy, R. Le Goc, O. Bour, and J. R. de Dreuzy (2009), Statistical methodology for Discrete Fracture Models - including fracture size, orientation uncertainty together with intensiy uncertainty and variability, 80 pp., Svensk Kärnbränslehantering AB.

Darot, M., and Y. Gueguen (1986), Slow crack growth in minerals and rocks: Theory and experiments, *Pure Appl. Geophys.*, 124(4-5), 677–692, doi:10.1007/bf00879604.

Das, S., and C. H. Scholz (1981), Theory of time-dependent rupture in the Earth, *J. Geophys. Res.*, 86(B7), 6039–6051, doi:10.1029/JB086iB07p06039.

Davy, P. (1993), On the frequency - length distribution of the San Andreas fault system, *J. Geophys. Res.*, 98(B7), 12141–12152, doi:10.1029/93JB00372.

Davy, P., A. Hansen, E. Bonnet, and S.-Z. Zhang (1995), Localization and fault growth in layered brittle-ductile systems: Implications for deformations of the continental lithosphere, *J. Geophys. Res.*, 100(B4), 6281–6294, 10.1029/94jb02983.

Davy, P., O. Bour, J. R. De Dreuzy, and C. Darcel (2006a), Flow in multiscale fractal fracture networks, in *Fractal Analysis for Natural Hazards*, pp. 31–45, edited by G. Cello, and B. D. Malamud, Geological Society of London, London.

Davy, P., C. Darcel, O. Bour, R. Munier, and J. R. d. Dreuzy (2006b), A note on the angular correction applied to fracture intensity profiles along drill core, *J. Geophys. Res.*, 111(B11), 1–7, doi:10.1029/2005jb004121.

Davy, P., R. L. Goc, C. Darcel, O. Bour, J. R. d. Dreuzy, and R. Munier (2010), A likely universal model of fracture scaling and its consequence for crustal hydromechanics, *J. Geophys. Res.*, 115(B10), 1–13, doi:10.1029/2009jb007043.

de Dreuzy, J.-R., P. Davy, and O. Bour (2001a), Hydraulic properties of two-dimensional random fracture networks following a power law length distribution 1. Effective connectivity, *Water Resour. Res.*, 37(8), 2065–2078, doi:10.1029/2001WR900011.

de Dreuzy, J.-R., P. Davy, and O. Bour (2001b), Hydraulic properties of two-dimensional random fracture networks following a power law length distribution 2. Permeability of networks based on lognormal distribution of apertures, *Water Resour. Res.*, 37(8), 2079–2096, doi:10.1029/2001WR900010.

de Dreuzy, J.-R., P. Davy, and O. Bour (2002), Hydraulic properties of two-dimensional random fracture networks following power law distributions of length and aperture, *Water Resour. Res.*, 38(12), 12-11–12-19, doi:10.1029/2001WR001009.

de Dreuzy, J.-R., P. d. Boiry, G. Pichot, and P. Davy (2010), Use of power averaging for quantifying the influence of structure organization on permeability upscaling in on-lattice networks under mean parallel flow, *Water Resour. Res.*, 46(8), 1–11, doi:10.1029/2009wr008769.

Dove, P. M. (1995), Geochemical controls on the kinetics of quartz fracture at subcritical tensile stresses, *J. Geophys. Res.*, 100(B11), 22349–22359.

Engelder, T. (1987), Joints and shear fractures in rock, in *Fracture Mechanics of Rock*, edited by B.K. Atkinson, pp. 27–69, Academic Press, London.

Erhel, J., J. R. De Dreuzy, and B. Poirriez (2009a), Flow simulation in three-dimensional discrete fracture networks, *SIAM J. Sci. Comput.*, 31(4), 2688–2705, doi:10.1137/080729244.

Erhel, J., J.-R. d. Dreuzy, A. Beaudoin, E. Bresciani, and D. Tromeur-Dervout (2009b), A parallel scientific software for heterogeneous hydrogeology in *Parallel CFD'2007*, 67.

Fox, A., P. La Pointe, J. Hermanson, and J. Öhman (2007), Statistical geological discrete fracture network model. Forsmark modelling stage 2.2, R-07-46, 1–271 pp., Svensk Kärnbränslehantering AB, Stockholm.

Griffith, A. A. (1920), The phenomena of rupture and flow in solids, *Philos. Trans. R. Soc. Lond. A*, 221, 163–198.

Hamiel, Y., O. Katz, V. Lyakhovsky, Z. Reches, and Y. Fialko (2006), Stable and unstable damage evolution in rocks with implications to fracturing of granite, *Geophys. J. Int.*, 167(2), 1005–1016.

Hansen, A., E. L. Hinrichsen, and S. Roux (1991), Scale-invariant disorder in fracture and related breakdown phenomena, *Phys. Rev. B*, *43*(1), 665–678.

Hardacre, K. M., and P. A. Cowie (2003), Controls on strain localization in a two-dimensional elastoplastic layer: Insights into size-frequency scaling of extensional fault populations, *J. Geophys. Res.*, *108*(B11), 15, doi:10.1029/2001jb001712.

Herrmann, H. J., and S. Roux (Eds.) (1990), *Statistical models for the fracture of disordered media*, 351 pp., North-Holland, Amsterdam.

Hoek, E., and E. T. Brown (1997), Practical estimates of rock mass strength, *Int. J. Rock Mech. Min. Sci.*, *34*(8), 1165–1186, doi:10.1016/s1365-1609 (97)80069-x.

Horii, H., and S. Nemat-Nasser (1985), Compression-induced microcrack growth in brittle solids: Axial Splitting and shear failure, *J. Geophys. Res.*, *90*(B4), 3105–3125, doi:10.1029/JB090iB04p03105.

Ingraffea, A. R. (1987), Theory of crack initiation and propagation in rock, in *Fracture Mechanics of Rock*, edited by B. K. Atkinson, pp. 71–110, Academic Press, London, Orlando.

Jing, L., and O. Stephansson (2007), Discrete Fracture Network (DFN) Method, in *Developments in Geotechnical Engineering*, edited by J. Lanru and S. Ove, pp. 365–398, Elsevier.

Josnin, J.-Y., H. Jourde, P. Fénart, and P. Bidaux (2002), A three-dimensional model to simulate joint networks in layered rocks, *Can. J. Earth Sci.*, *39*(10), 1443–1455, doi:10.1139/e02-043.

Kachanov, M., and J. P. Laures (1989), Three-dimensional problems of strongly interacting arbitrarily located penny-shaped cracks, *Int. J. Fract.*, *41*(4), 289–313.

Kachanov, M. (2003), On the problems of crack interactions and crack coalescence, *Int. J. Fract.*, *120*(3), 537–543, doi:10.1023/a:1025448314409.

Kamaya, M., and T. Kitamura (2004), A simulation on growth of multiple small cracks under stress corrosion, *Int. J. Fract.*, *V130*(4), 787–801.

Knauss, W. (1969), Stable and unstable crack growth in viscoelastic media, *Trans. Soc. Rheol.*, *13*(3), 291–313.

Ko, T. Y., and J. Kemeny (2011), Subcritical crack growth in rocks under shear loading, *J. Geophys. Res.*, *116*(B1), B01407.

Korvin, G. (1989), Fractured but not fractal: Fragmentation of the gulf of suez basement, *Pure Appl. Geophys.*, *131*(1), 289–305.

Kranz, R. L. (1983), Microcracks in rocks: A review, *Tectonophysics*, *100* (1-3), 449–480.

La Pointe, P., A. Fox, J. Hermanson, and J. Öhman (2008), Geological discrete fracture network model for the Laxemar site. Site Descriptive Modelling -Site Laxemar, *R-08-55*, 1-260 pp, Svensk Kärnbränslehantering AB, Stockholm.

Malthe-Sørenssen, A., T. Walmann, J. Feder, T. Jøssang, P. Meakin, and H. H. Hardy (1998), Simulation of extensional clay fractures, *Phys. Rev. E*, *58*(5), 5448–5564.

Newman Jr, J. C., and I. S. Raju (1981), An empirical stress-intensity factor equation for the surface crack, *Eng. Fract. Mech.*, *15*(1–2), 185–192, doi:10.1016/0013-7944(81)90116-8.

Nur, A. (1982), The origin of tensile fracture lineaments, *J. Struct. Geol.*, *4* (1), 31–40.

Odling, N. E. (1997), Scaling and connectivity of joint systems in sandstones from western Norway, *J. Struct. Geol.*, *19*(10), 1257–1271, doi:10.1016/S0191-8141(97)00041-2.

Olson, J. E. (1993), Joint pattern development: Effects of subcritical crack growth and mechanical crack interaction, *J. Geophys. Res.*, *98*(B7), 12251–12265, doi:10.1029/93jb00779.

Olson, J. E. (2003), Sublinear scaling of fracture aperture versus length: An exception or the rule?, *J. Geophys. Res.*, *108*, doi:10.1029/2001jb000419.

Olson, J. E. (2004), Predicting fracture swarms — the influence of subcritical crack growth and the crack-tip process zone on joint spacing in rock, in *The Initiation, Propagation, and Arrest of Joins and Other Fractures*, edited by J. W. Cosgrove, and T. Engelder, Geological Society, London, 73-88.

Olson, J. E., and R. A. Schultz (2011), Comment on "A note on the scaling relations for opening mode fractures in rock" by C.H. Scholz, *J. Struct. Geol.*, *33*(10), 1523–1524, doi:10.1016/j.jsg.2011.07.004.

Paluszny, A., and S. K. Matthai (2010), Impact of fracture development on the effective permeability of porous rocks as determined by 2-D discrete fracture growth modeling, *J. Geophys. Res.*, *115*(B2), B02203, doi:10.1029/2008jb006236.

Pichot, G., J. Erhel, and J. R. De Dreuzy (2010), A mixed hybrid Mortar method for solving flow in discrete fracture networks, *Appl. Anal.*, *89* (10), 1629–1643.

Piggott, A. (1997), Fractal relations for the diameter and trace length of disc-shaped fractures, *J. Geophys. Res.*, *102*(B8), 18121–128126.

Pollard, D. D., and A. Aydin (1988), Progress in understanding jointing over the past century, *Geol. Soc. Am. Bull.*, *100*(8), 1181–1204, doi:10.1130/0016-7606(1988)100<1181:piujot>2.3.co;2.

Reches, Z. e., and D. A. Lockner (1994), Nucleation and growth of faults in brittle rocks, *J. Geophys. Res.*, *99*(B9), 18159–18173, doi:10.1029/94jb00115.

Renshaw, C. E., and D. D. Pollard (1994), Numerical simulation of fracture set formation: A fracture mechanics model consistent with experimental observations, *J. Geophys. Res.*, *99*(B5), 9359–9372.

Renshaw, C. E. (1996), Influence of subcritical fracture growth on the connectivity of fracture networks, *Water Resour. Res.*, *32*(6), 1519–1530.

Renshaw, C. E., and J. C. Park (1997), Effect of mechanical interactions on the scaling of fracture length and aperture, *Nature*, *386*, 482–484.

Renshaw, C. E., T. A. Myse, and S. R. Brown (2003), Role of heterogeneity in elastic properties and layer thickness in the jointing of layered sedimentary rocks, *Geophys. Res. Lett.*, *30*(24), 4, doi:10.1029/2003gl018489.

Sano, O., I. Ito, and M. Terada (1981), Influence of strain rate on dilatancy and strength of Oshima granite under uniaxial compression, *J. Geophys. Res.*, *86*(B10), 9299–9311, doi:10.1029/JB086iB10p09299.

Scholz, C. H. (2010), A note on the scaling relations for opening mode fractures in rock, *J. Struct. Geol.*, *32*(10), 1485–1487, doi:10.1016/j.jsg.2010.09.007.

Schultz, R. A. (2000), Growth of geologic fractures into large-strain populations: Review of nomenclature, subcritical crack growth, and some implications for rock engineering, *Int. J. Rock Mech. Min. Sci.*, *37*(1-2), 403–411.

Segall, P., and D. D. Pollard (1983), Joint formation in granitic rock of the Sierra Nevada, *Geol. Soc. Am. Bull.*, *94*(5), 563–575, doi:10.1130/0016-7606.

Segall, P. (1984a), Rate-dependent extensional deformation resulting from crack growth in rock, *J. Geophys. Res.*, *89*(B6), 4185–4195, doi:10.1029/JB089iB06p04185.

Segall, P. (1984b), Formation and growth of extensional fracture sets, *Geol. Soc. Am. Bull.*, *95*(4), 454–462, doi:10.1130/0016-7606(1984)95<454:fagoef>2.0.co;2.

Sethna, J. P. (2001), Formal considerations about fracture: Nucleation and growth, *arXiv preprint cond-mat/0102535*.

SKB (2004a), Preliminary site description Forsmark area - version 1.1, Svensk Kärnbränslehantering, A. B., Stockholm.

SKB (2004b), Preliminary site description. Simpevarp area - version 1.1, Svensk Kärnbränslehantering, A. B., Stockholm.

Sornette, D., and P. Davy (1991), Fault growth model and the universal fault length distribution, *Geophys. Res. Lett.*, *18*(6), 1079–1081, doi:10.1029/91gl01054.

Spyropoulos, C., W. J. Griffith, C. H. Scholz, and B. E. Shaw (1999), Experimental evidence for different strain regimes of crack populations in a clay model, *Geophys. Res. Lett.*, *26*, doi:10.1029/1999gl900175.

Stephens, M. B., et al. (2008), Geology Forsmark. Site descriptive modelling Forsmark stage 2.2, *R-07-45*, 1–224 pp, Svensk Kärnbränslehantering AB, Stockholm.

Svensson, U. (2001), A continuum representation of fracture networks. Part II: Application to the Äspö Hard Rock laboratory. *J. Hydrol.*, *250*(1), 187–205.

Tapponnier, P., and W. Brace (1976), Development of stress-induced microcracks in Westerly granite, *International Journal of Rock Mechanics and Mining Sciences & Geomechanics Abstracts*, *13*(4), 103–112, doi:10.1016/0148-9062(76)91937-9.

Tchalenko, J. S. (1970), Similarities between shear zones of different magnitudes, *Geol. Soc. Am. Bull.*, *81*(6), 1625–1640, doi:10.1130/0016-7606 (1970)81[1625:sbszod]2.0.co;2.

Vanel, L., S. Ciliberto, P.-P. Cortet, and S. Santucci (2009), Time-dependent rupture and slow crack growth: Elastic and viscoplastic dynamics, *J. Phys. D: Appl. Phys.*, *42*(21), 214007.

Vermilye, J. M., and C. H. Scholz (1998), The process zone: A microstructural view of fault growth, *J. Geophys. Res.*, *103*(B6), 12223–12237, doi:10.1029/98jb00957.

Wahlgren, C.-H., et al. (2008), Geology Laxemar. Site descriptive modelling SDM-Site Laxemar, *R-08-54*, Svensk Kärnbränslehantering AB, Stockholm.

Walsh, J. J., A. Nicol, and C. Childs (2002), An alternative model for the growth of faults, *J. Struct. Geol.*, *24*(11), 1669–1675, doi:10.1016/s0191-8141(01)00165-1.

Zapperi, S., and P. K. V. V. Nukala (2006), Fracture statistics in the three-dimensional random fuse model, *Int. J. Fract.*, *V140*(1), 99–111.